SCIENTIFIC REPORTS

OPEN

# A widespread internal resonance phenomenon in functionally graded material plates with longitudinal speed

Received: 17 August 2018
Accepted: 15 December 2018
Published online: 13 February 2019

Y. F. Zhang & J. T. Liu

**A widespread internal resonance phenomenon is detected in axially moving functionally graded material (FGM) rectangular plates. The geometrical nonlinearity is taken into account with the consideration of von Kármán nonlinear geometric equations. Using d'Alembert's principle, governing equation of the transverse motion is derived. The obtained equation is further discretized to ordinary differential equations using the Galerkin technique. The harmonic balance method is adopted to solve the above equations. Additionally, stability analysis of steady-state solutions is presented. Research shows that a one-to-one internal resonance phenomenon widely exists in a large range of constituent volume distribution in moving FGM plates. Moreover, it is found that this internal resonance phenomenon can easily happen even though the FGM plates are under extremely small external excitation or with very large damping.**

In order to meet the demanding requirements for comprehensive behavior of engineering structures in modern industries, a group of Japanese materials researchers composed a new type of non-uniform composite materials in the mid-1980s, namely, functional Gradient Materials (FGMs)[1]. The advantage of FGMs is that physical properties have no mutation in the materials. In recent years, FGM structures have been widely applied in defense industry, ships, aerospace and other high-tech fields. Therefore, the mechanical behavior analysis of FGM structures has attracted increasing attention.

In practical applications, FGM plates are usually important structural element. Dynamics investigation of FGM plates plays significant role in structure design. However, dynamics analyses of FGM plates are still not large[2–4]. Among them, some studies were carried out on *linear* dynamics of FGM plates[5–7]. On the other hand, literature on *nonlinear* dynamics of FGM plates is very limited. Wang and coauthors analyzed imperfection and piezoelectricity effect on non-linear behavior of FGM plates[8,9]. Hao *et al.*[10] presented nonlinear vibration study of FGM plates; quasi periodic, periodic and chaotic vibrations were mainly discussed. Nonlinear vibrations of embedded FGM plates was discussed by Duc *et al.*[11] based on the Runge-Kutta method. Based on the Lagrange method, Alijani *et al.*[12] studied nonlinear dynamics of FGM plates using pseudo-arc-length continuation technique. Wang and Zu[13] presented broadband vibration of traveling piezoelectric FGM plates. Zhang *et al.*[14] discussed chaotic vibration of shear deformable FGM plates employing the technique of multiple scales. Adopting single-mode approximation, Allahverdizadeh *et al.*[15] analyzed the existence condition of periodic solutions to FGM plates. FGM plates with cracks were considered by Yang *et al.*[16], who discussed nonlinear frequencies and transient response of the structure. Recently, using the classical plate theory, Wang and Zu[17] considered non-linear steady-state response of moving FGM plates in fluid.

Structural internal resonance is a unique nonlinear phenomenon in engineering system. If any of the natural frequencies of structures are commensurable, internal resonance can occur. In this condition, mode interaction becomes strong, and hence, significant. The system energy is continuously converted between the two coupled modes, and the amplitude and phase change periodically. Thus, understanding the mechanism of internal resonance in structural elements such as beams, plates and shells is of importance for the design and application of these structures. Some studies have focused on the internal resonance phenomenon in these structures, for

College of Aerospace Engineering, Shenyang Aerospace University, Shenyang, 110136, China. Correspondence and requests for materials should be addressed to Y.F.Z. (email: yufeizhang73@163.com)

example, internal resonance in metal plates[18], beams[19], cylindrical shells[20], fluid-conveying pipes[21], and strips and strings[22].

Longitudinally moving continuums have attracted much attention in the past twenty years owing to their broad spectrum of use in various engineering fields such as robotic manipulators, extrusion processes, and so on. One-dimensional longitudinally moving continuums including strings, belts and beams have been widely investigated[23–30]. Two-dimensional longitudinally moving continuums such as plates were also studied[31,32]. Hatami *et al.*[33] studied natural frequencies of longitudinally moving viscoelastic plates by utilizing the method of finite strip. Wang and Zu[34] carried out analytical study on free vibration of traveling plates immerged in liquid. Banichuk *et al.*[35] studied the stability of traveling plates with a constant speed; their concentration was focused on transverse vibration of the plates. Marynowski[36] carried out linear dynamics study on longitudinally traveling viscoelastic plates of Levy type. Wang *et al.*[37–39] studied deeply dynamic characteristics of moving plates with fluid-structure interaction.

Literature review indicates that research on dynamics of longitudinally moving plates was mainly focused on *metal* plates. This paper studies dynamic characteristics of longitudinally moving FGM plates, and attention is particularly focused on the internal resonance behavior. On the base of d'Alembert's principle, mathematical model of the system is developed by taking into account geometrical nonlinearity of von Kármán type. The obtained model is further discretized to ordinary differential equations using the Galerkin technique. The harmonic balance method is adopted to solve these equations. This study retains all original physical quantities in the parametric study, thus allowing intuitive understanding of physical parameter effects on the internal resonance behavior.

## Mathematical Modeling

Consider a thin rectangular FGM plate made of stainless steel and nickel, which is simply supported at all edges and axially travels with a constant velocity $V$, as seen in Fig. 1a. The plate has the thickness $h$, width $b$ and length $a$. A coordinate system is established with the origin $O$ locating at the corner of the plate. Let $u$, $v$ and $w$ represent displacements of the plate mid-plane along $x$-, $y$- and $z$- axes from static equilibrium ($u=v=w=0$), respectively. The forces and moments acting on a plate element are presented in Fig. 1b. For simplification, the infinitesimal plate element is represented by its middle surface. Additionally, a tension per unit width along the $x$-axis, denoted by $N_0$, is loaded on the plate.

For a FGM plate, its effective material properties are written as[40,41]:

$$P(z) = P_{Ni}\, V_{Ni}(z) + P_S\, V_S(z) \tag{1}$$

in which $P_S$ and $P_{Ni}$ are material properties of stainless steel and nickel, respectively; $V_S$ and $V_{Ni}$ denote volume fractions of stainless steel and nickel, respectively.

The relation between both volume fractions should be

$$V_{Ni} + V_S = 1 \tag{2}$$

The constituent volume fraction is considered to vary smoothly along the $z$-axis and satisfy power law distribution. For nickel, it is given by

$$V_S(z) = \left(\frac{z}{h} + \frac{1}{2}\right)^N \tag{3}$$

where $N \in [0, \infty)$ denote the power-law exponent.

Therefore, the general mass density $\rho(z)$, Young's modulus $E(z)$ and Poisson's ratio $\mu(z)$ of the FGM plate are

$$\mu(z) = (\mu_S - \mu_{Ni})\left(\frac{z}{h} + \frac{1}{2}\right)^N + \mu_{Ni} \tag{4}$$

$$E(z) = (E_S - E_{Ni})\left(\frac{z}{h} + \frac{1}{2}\right)^N + E_{Ni} \tag{5}$$

$$\rho(z) = (\rho_S - \rho_{Ni})\left(\frac{z}{h} + \frac{1}{2}\right)^N + \rho_{Ni} \tag{6}$$

According to the classical thin plate theory, we have[42]

$$\varepsilon_x = \varepsilon_x^0 + z\chi_x, \quad \varepsilon_y = \varepsilon_y^0 + z\chi_y, \quad \gamma_{xy} = \gamma_{xy}^0 + 2z\chi_{xy} \tag{7}$$

where $\varepsilon_x$, $\varepsilon_y$ and $\gamma_{xy}$ denote strains of an arbitrary point, $\chi_{xy}$, $\chi_y$ and $\chi_x$ the torsion and curvature changes of middle plane, $\varepsilon_x^0$, $\varepsilon_y^0$ and $\gamma_{xy}^0$ the mid-plane strains, $z$ the distance of an arbitrary point to the mid-plane.

Geometric relations of the von Kármán nonlinear theory are[43,44]

$$\left\{\varepsilon_x^0,\ \varepsilon_y^0,\ \gamma_{xy}^0\right\} = \left\{\frac{\partial u}{\partial x} + \frac{1}{2}\left(\frac{\partial w}{\partial x}\right)^2,\ \frac{\partial v}{\partial y} + \frac{1}{2}\left(\frac{\partial w}{\partial y}\right)^2,\ \frac{\partial v}{\partial x} + \frac{\partial u}{\partial y} + \frac{\partial w}{\partial x}\frac{\partial w}{\partial y}\right\} \tag{8}$$

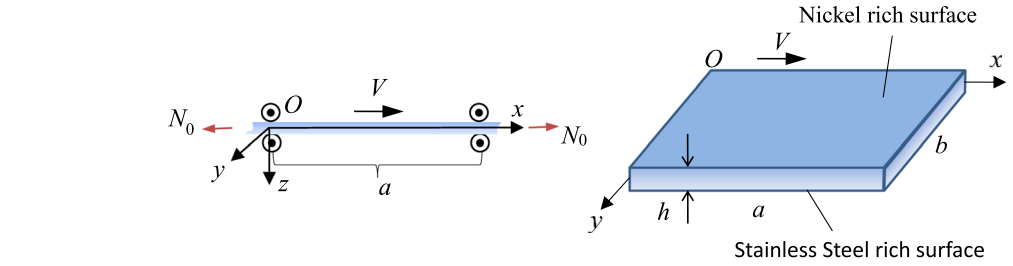


(a)

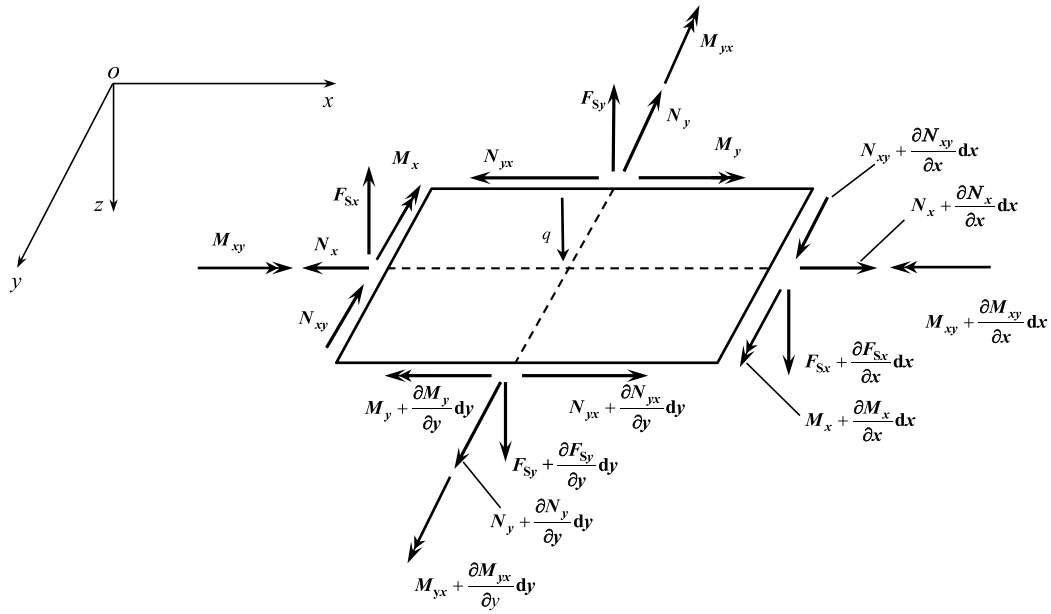


(b)

**Figure 1.** Schematic of moving FGM plate: (**a**) geometry and coordinate system; (**b**) Forces and moments acting on a plate element.

$$\{\chi_x,\ \chi_y,\ \chi_{xy}\} = \left\{-\frac{\partial^2 w}{\partial x^2},\ -\frac{\partial^2 w}{\partial y^2},\ -\frac{\partial^2 w}{\partial x \partial y}\right\} \tag{9}$$

For a FGM plate, stress-strain relationships are given by

$$\boldsymbol{\sigma} = \mathbf{Q} \cdot \boldsymbol{\varepsilon} \tag{10}$$

where

$$\boldsymbol{\sigma}^{\mathrm{T}} = [\sigma_x \quad \sigma_y \quad \tau_{xy}], \quad \mathbf{Q} = \begin{bmatrix} Q_{11} & Q_{12} & 0 \\ Q_{21} & Q_{22} & 0 \\ 0 & 0 & Q_{66} \end{bmatrix}, \quad \boldsymbol{\varepsilon}^{\mathrm{T}} = [\varepsilon_x \quad \varepsilon_y \quad \gamma_{xy}] \tag{11}$$

in which $\tau_{xy}$ stands for in-plane shear stress, $\sigma_x$ and $\sigma_y$ the normal stresses, $Q_{ij}$ $(i, j = 1, 2, 6)$ the reduced stiffness components.

Reduced stiffnesses are expressed as:

$$Q_{11} = Q_{22} = \frac{E(z)}{[1 - \mu(z)^2]} \tag{12}$$

$$Q_{12} = Q_{21} = \frac{E(z) \cdot \mu(z)}{[1 - \mu(z)^2]} \tag{13}$$

$$Q_{66} = \frac{E(z)}{2[1 + \mu(z)]} \tag{14}$$

The resultant forces and moments of the FGM plate take the form of[42,45]

$$\begin{bmatrix} N_x \\ N_y \\ N_{xy} \end{bmatrix} = \int_{-h/2}^{h/2} \begin{bmatrix} \sigma_x \\ \sigma_y \\ \tau_{xy} \end{bmatrix} \mathrm{d}z \tag{15}$$

$$\begin{bmatrix} M_x \\ M_y \\ M_{xy} \end{bmatrix} = \int_{-h/2}^{h/2} \begin{bmatrix} \sigma_x \\ \sigma_y \\ \tau_{xy} \end{bmatrix} z\mathrm{d}z \tag{16}$$

Substituting Eqs (7) and (10) in Eqs (15) and (16) leads to the constitutive relations

$$\mathbf{N} = \mathbf{S} \cdot \boldsymbol{\varepsilon} \tag{17}$$

with

$$\mathbf{N}^{\mathrm{T}} = [N_x \quad N_y \quad N_{xy} \quad M_x \quad M_y \quad M_{xy}] \tag{18}$$

$$\boldsymbol{\varepsilon}^{\mathrm{T}} = \left[\varepsilon_x^0 \quad \varepsilon_y^0 \quad \gamma_{xy}^0 \quad \chi_x \quad \chi_y \quad \chi_{xy}\right] \tag{19}$$

and

$$\mathbf{S} = \begin{bmatrix} A_{11} & A_{12} & 0 & B_{11} & B_{12} & 0 \\ A_{12} & A_{22} & 0 & B_{12} & B_{22} & 0 \\ 0 & 0 & A_{66} & 0 & 0 & B_{66} \\ B_{11} & B_{12} & 0 & D_{11} & D_{12} & 0 \\ B_{12} & B_{22} & 0 & D_{12} & D_{22} & 0 \\ 0 & 0 & B_{66} & 0 & 0 & D_{66} \end{bmatrix} \tag{20}$$

in which $A_{ij}$, $B_{ij}$ and $D_{ij}$ $(i, j = 1, 2, 6)$ denote stiffness coefficients. Their expressions take the form

$$A_{ij} = \int_{-h/2}^{h/2} Q_{ij}\mathrm{d}z \tag{21}$$

$$B_{ij} = \int_{-h/2}^{h/2} Q_{ij}z\mathrm{d}z \tag{22}$$

$$D_{ij} = \int_{-h/2}^{h/2} Q_{ij}z^2\mathrm{d}z \tag{23}$$

On the base of the d'Alembert principle, we can derive the dynamic equilibrium equation governing the transverse vibration of a moving FGM plate:

$$\begin{aligned} &\int_{-\frac{h}{2}}^{\frac{h}{2}} \rho\frac{\mathrm{d}^2w}{\mathrm{d}t^2}\mathrm{d}z - \frac{\partial^2 M_x}{\partial x^2} - 2\frac{\partial^2 M_{xy}}{\partial x\partial y} - \frac{\partial^2 M_y}{\partial y^2} - (N_x + N_0)\frac{\partial^2 w}{\partial x^2} \\ &\quad - N_y\frac{\partial^2 w}{\partial y^2} - 2N_{xy}\frac{\partial^2 w}{\partial x\partial y} + c\left(\frac{\partial w}{\partial t} + V\frac{\partial w}{\partial x}\right) + F(x, y, t) = 0 \end{aligned} \tag{24}$$

in which $c$ stands for damping coefficient.

The derivative of the first term in Eq. (24) takes the form

$$\frac{\mathrm{d}^2w}{\mathrm{d}t^2} = \frac{\partial^2 w}{\partial t^2} + 2V\frac{\partial^2 w}{\partial x\partial t} + V^2\frac{\partial^2 w}{\partial x^2} \tag{25}$$

The transverse external excitation $F(x, y, t)$ in Eq. (24) is harmonic point load

$$F(x, y, t) = F_0\cos(\omega t)\delta(x - x_0)\delta(y - y_0) \tag{26}$$

in which $\delta$ and $F_0$ denote Dirac delta function and force amplitude, respectively, $\omega$ the excitation frequency, $x_0$ and $y_0$ the in-plane coordinates. The load is applied at $x_0 = a/2$ and $y_0 = b/2$ in this study.

Employing Eqs (7), (10), (15 and 16), (25) and (26) in Eq. (24) gives the governing equation in term of $w$

$$
\begin{aligned}
&D_{11}\frac{\partial^4 w}{\partial x^4} + (2D_{12} + 4D_{66})\frac{\partial^4 w}{\partial x^2 \partial y^2} + D_{22}\frac{\partial^4 w}{\partial y^4} - N_0\frac{\partial^2 w}{\partial x^2} + c\left(\frac{\partial w}{\partial t} + V\frac{\partial w}{\partial x}\right)\\
&+ \int_{-\frac{h}{2}}^{\frac{h}{2}} \rho\left(\frac{\partial^2 w}{\partial t^2} + 2V\frac{\partial^2 w}{\partial x \partial t} + V^2\frac{\partial^2 w}{\partial x^2}\right)\mathrm{d}z - 2A_{66}\frac{\partial w}{\partial x}\frac{\partial w}{\partial y}\frac{\partial^2 w}{\partial x \partial y}\\
&+ \frac{1}{2}(4B_{66} - 4B_{12})\left(\frac{\partial^2 w}{\partial x \partial y}\right)^2 + \frac{1}{2}(-2B_{12} - 4B_{66})\frac{\partial w}{\partial x}\frac{\partial^3 w}{\partial x \partial y^2}\\
&+ \frac{1}{2}(4B_{12} - 4B_{66})\frac{\partial^2 w}{\partial x^2}\frac{\partial^2 w}{\partial y^2} + \frac{1}{2}(-2B_{12} - 4B_{66})\frac{\partial w}{\partial y}\frac{\partial^3 w}{\partial x^2 \partial y}\\
&+ \frac{1}{2}\Bigg[-A_{22}\frac{\partial^2 w}{\partial y^2}\left(\frac{\partial w}{\partial y}\right)^2 - A_{12}\frac{\partial^2 w}{\partial x^2}\left(\frac{\partial w}{\partial y}\right)^2 - A_{12}\frac{\partial^2 w}{\partial y^2}\left(\frac{\partial w}{\partial x}\right)^2\\
&- A_{11}\left(\frac{\partial w}{\partial x}\right)^2\frac{\partial^2 w}{\partial x^2} - 2B_{22}\frac{\partial^3 w}{\partial y^3}\frac{\partial w}{\partial y} - 2B_{11}\frac{\partial w}{\partial x}\frac{\partial^3 w}{\partial x^3}\Bigg]\\
&+ F_0\cos(\omega t)\delta(x - x_0)\delta(y - y_0) = 0
\end{aligned}
\tag{27}
$$

in which shear and normal stress components are neglected[46].

## Approximate Analytical Solutions

In this study, we focus on the one-to-one internal resonance between the first two modes. Accordingly, the displacement that exactly satisfies the simply supported boundary condition is given by

$$
w(x, y, t) = A_{\overline{m},\overline{n}}(t)\sin\left(\frac{\overline{m}\pi x}{a}\right)\sin\left(\frac{\overline{n}\pi y}{b}\right) + A_{\overline{j},\overline{k}}(t)\sin\left(\frac{\overline{j}\pi x}{a}\right)\sin\left(\frac{\overline{k}\pi y}{b}\right) \tag{28}
$$

where $\overline{m}$, $\overline{j}$, $\overline{n}$ and $\overline{k}$ denote the mode numbers; $A_{\overline{m},\overline{n}}(t)$ and $A_{\overline{j},\overline{k}}(t)$ stand for generalized coordinates with respect to time $t$.

Using the Galerkin method, the weight functions are given by

$$
F_p(x, y) = \begin{cases} \sin(\overline{m}\pi x/a)\sin(\overline{n}\pi y/b) & p = 1 \\ \sin(\overline{j}\pi x/a)\sin(\overline{k}\pi y/b) & p = 2 \end{cases} \tag{29}
$$

The Galerkin procedure takes the form of

$$
\left\langle Eq.\ (27),\ \ F_p \right\rangle = \int_0^b \int_0^a Eq.\ (27)\ F_p(x, y)\,\mathrm{d}x\,\mathrm{d}y \tag{30}
$$

The derivation of Eq. (30) can be performed with the aid of *Mathematica* software[47]. Thus, we can derive the following nonlinear ordinary differential equations related to $A_{\overline{m},\overline{n}}(t)$ and $A_{\overline{j},\overline{k}}(t)$:

$$
\begin{cases}
\ddot{A}_{\overline{m},\overline{n}}(t) + \overline{M}_1\dot{A}_{\overline{m},\overline{n}}(t) + \overline{M}_2\dot{A}_{\overline{j},\overline{k}}(t) + \overline{M}_3 A_{\overline{m},\overline{n}}(t) + \overline{M}_4 A_{\overline{j},\overline{k}}(t)\\
\quad + \overline{M}_5 A^3_{\overline{m},\overline{n}}(t) + \overline{M}_6 A_{\overline{m},\overline{n}}(t)A^2_{\overline{j},\overline{k}}(t) + \overline{M}_7 A^2_{\overline{m},\overline{n}}(t) + \overline{M}_8 A^2_{\overline{j},\overline{k}}(t) + \overline{M}_9\cos(\omega t) = 0\\
\ddot{A}_{\overline{j},\overline{k}}(t) + \overline{S}_1\dot{A}_{\overline{m},\overline{n}}(t) + \overline{S}_2\dot{A}_{\overline{j},\overline{k}}(t) + \overline{S}_3 A_{\overline{m},\overline{n}}(t)\\
\quad + \overline{S}_4 A_{\overline{j},\overline{k}}(t) + \overline{S}_5 A^3_{\overline{j},\overline{k}}(t) + \overline{S}_6 A^2_{\overline{m},\overline{n}}(t)A_{\overline{j},\overline{k}}(t) + \overline{S}_7 A_{\overline{m},\overline{n}}(t)A_{\overline{j},\overline{k}}(t) = 0
\end{cases} \tag{31}
$$

in which the over-dot stands for derivative to time; $\overline{M}_i$ and $\overline{S}_j$ ($i = 1, 2, \ldots, 9, j = 1, 2, \ldots, 7$) denote proper parameters which are presented in Appendix.

Introduce non-dimensional variables as follows

$$
\tau = \omega_{\overline{m},\overline{n}}t, \quad \Omega = \omega/\omega_{\overline{m},\overline{n}}, \quad q_1(\tau) = A_{\overline{m},\overline{n}}(t)/h, \quad q_2(\tau) = A_{\overline{j},\overline{k}}(t)/h \tag{32}
$$

where $\omega_{\overline{m},\overline{n}}$ is the fundamental natural frequency.

Employing Eq. (32) in Eq. (31) gives non-dimensional equations:

$$
\begin{cases}
\ddot{q}_1(\tau) = M_1\dot{q}_1(\tau) + M_2\dot{q}_2(\tau) + M_3 q_1(\tau) + M_4 q_2(\tau) + M_5 q_1^3(\tau)\\
\qquad + M_6 q_1(\tau)q_2^2(\tau) + M_7 q_1^2(\tau) + M_8 q_2^2(\tau) + M_9\cos(\Omega\tau)\\
\ddot{q}_2(\tau) = S_1\dot{q}_1(\tau) + S_2\dot{q}_2(\tau) + S_3 q_1(\tau) + S_4 q_2(\tau)\\
\qquad + S_5 q_2^3(\tau) + S_6 q_1^2(\tau)q_2(\tau) + S_7 q_1(\tau)q_2(\tau)
\end{cases} \tag{33}
$$

where $M_i$ and $S_j$ ($i = 1, 2, \ldots, 9, j = 1, 2, \ldots, 7$) denote proper coefficients deriving from the dimensionless transformation.

According to the harmonic balance method, the solutions of Eq. (33) can be expressed as

$$q_1(\tau) = A_0 + \sum_{n=1}^{H}[A_{2n-1}\cos(n\Omega\tau) + A_{2n}\sin(n\Omega\tau)] \tag{34}$$

$$q_2(\tau) = B_0 + \sum_{n=1}^{H}[B_{2n-1}\cos(n\Omega\tau) + B_{2n}\sin(n\Omega\tau)] \tag{35}$$

in which $A_n$ and $B_n$ ($n=0, 1, \ldots, H$) denote Fourier's coefficients.

The time derivatives are expressed as

$$\dot{q}_1(\tau) = \sum_{n=1}^{H}[-n\Omega A_{2n-1}\sin(n\Omega\tau) + n\Omega A_{2n}\cos(n\Omega\tau)] \tag{36}$$

$$\dot{q}_2(\tau) = \sum_{n=1}^{H}[-n\Omega B_{2n-1}\sin(n\Omega\tau) + n\Omega B_{2n}\cos(n\Omega\tau)] \tag{37}$$

$$\ddot{q}_1(\tau) = \sum_{n=1}^{H}[-n^2\Omega^2 A_{2n-1}\cos(n\Omega\tau) - n^2\Omega^2 A_{2n}\sin(n\Omega\tau)] \tag{38}$$

$$\ddot{q}_2(\tau) = \sum_{n=1}^{H}[-n^2\Omega^2 B_{2n-1}\cos(n\Omega\tau) - n^2\Omega^2 B_{2n}\sin(n\Omega\tau)] \tag{39}$$

Introducing Eqs (34–39) in Eq. (33) and extracting each harmonic terms, one can obtain $4H+2$ algebraic equations related to $A_n$ and $B_n$ ($n=0, 1, \ldots, H$). Setting $H=1$, we have

$$\begin{cases} Fun_1(A_0, B_0, A_1, B_1, A_2, B_2, \Omega) = 0 \\ Fun_2(A_0, B_0, A_1, B_1, A_2, B_2, \Omega) = 0 \\ Fun_3(A_0, B_0, A_1, B_1, A_2, B_2, \Omega) = 0 \\ Fun_4(A_0, B_0, A_1, B_1, A_2, B_2, \Omega) = 0 \\ Fun_5(A_0, B_0, A_1, B_1, A_2, B_2, \Omega) = 0 \\ Fun_6(A_0, B_0, A_1, B_1, A_2, B_2, \Omega) = 0 \end{cases} \tag{40}$$

in which $Fun_i$ ($i=1, 2, \ldots, 6$) are expressions with respect to $A_0$, $B_0$, $A_1$, $B_1$, $A_2$, $B_2$ and $\Omega$. Eq. (40) is very expatiatory and the forms of $Fun_i$ are omitted here. From Eq. (40), one can obtain $A_0$, $B_0$, $A_1$, $B_1$, $A_2$, $B_2$ for a given $\Omega$; substituting the results in Eqs (34) and (35) gives the solutions of $q_1$ and $q_2$.

## Stability of Steady State Analytical Solutions

For the purpose of analyzing the stability of steady state solutions, the following coordinate transformations are introduced:

$$q_1(\tau) = A_0 + \Delta A_0(\tau) + [A_1 + \Delta A_1(\tau)]\cos(\Omega\tau) + [A_2 + \Delta A_2(\tau)]\sin(\Omega\tau) \tag{41}$$

$$q_2(\tau) = B_0 + \Delta B_0(\tau) + [B_1 + \Delta B_1(\tau)]\cos(\Omega\tau) + [B_2 + \Delta B_2(\tau)]\sin(\Omega\tau) \tag{42}$$

where $\Delta A_i(\tau)$ and $\Delta B_i(\tau)$ ($i=0, 1, 2$) mean perturbations.

Substituting Eqs (41 and 42) in Eq. (33), one may get a series of disturbance equations relating to $\Delta A_i(\tau)$ and $\Delta B_i(\tau)$ ($i=0, 1, 2$). Their expressions are given by

$$\dot{\mathbf{a}} = \mathbf{f}(\mathbf{a}, \mathbf{s}, \tau) \tag{43}$$

where

$$\begin{aligned}\mathbf{a} = [&\Delta A_0(\tau)\ \ \Delta\dot{A}_0(\tau)\ \ \Delta B_0(\tau)\ \ \Delta\dot{B}_0(\tau)\ \ \Delta A_1(\tau)\ \ \Delta\dot{A}_1(\tau)\\ &\Delta B_1(\tau)\ \ \Delta\dot{B}_1(\tau)\ \ \Delta A_2(\tau)\ \ \Delta\dot{A}_2(\tau)\ \ \Delta B_2(\tau)\ \ \Delta\dot{B}_2(\tau)]^{\mathrm{T}}\end{aligned} \tag{44}$$

$$\mathbf{s} = [A_0\ \ B_0\ \ A_1\ \ B_1\ \ A_2\ \ B_2]^{\mathrm{T}} \tag{45}$$

$$\begin{aligned}\mathbf{f} = [&f_1(\mathbf{a}, \mathbf{s}, \tau)\ \ f_2(\mathbf{a}, \mathbf{s}, \tau)\ \ f_3(\mathbf{a}, \mathbf{s}, \tau)\ \ f_4(\mathbf{a}, \mathbf{s}, \tau)\ \ f_5(\mathbf{a}, \mathbf{s}, \tau)\ \ f_6(\mathbf{a}, \mathbf{s}, \tau)\\ &f_7(\mathbf{a}, \mathbf{s}, \tau)\ \ f_8(\mathbf{a}, \mathbf{s}, \tau)\ \ f_9(\mathbf{a}, \mathbf{s}, \tau)\ \ f_{10}(\mathbf{a}, \mathbf{s}, \tau)\ \ f_{11}(\mathbf{a}, \mathbf{s}, \tau)\ \ f_{12}(\mathbf{a}, \mathbf{s}, \tau)]^{\mathrm{T}}\end{aligned} \tag{46}$$

At $\mathbf{a}=\mathbf{0}$, performing Taylor series expansion to $\mathbf{f}$ yields

| *N* | Present | Ref.[12] |
|---|---|---|
| Ceramic | 13.175 | 13.173 |
| 0.5 | 9.111 | 9.068 |
| 1 | 7.985 | 7.948 |
| 2 | 7.205 | 7.140 |
| Metal | 5.699 | 5.698 |

**Table 1.** Comparison of frequency parameter $\omega^* = \omega a^2/h\sqrt{\rho_m(1-\mu^2)/E_m}$ for stationary FGM plate at room temperature.

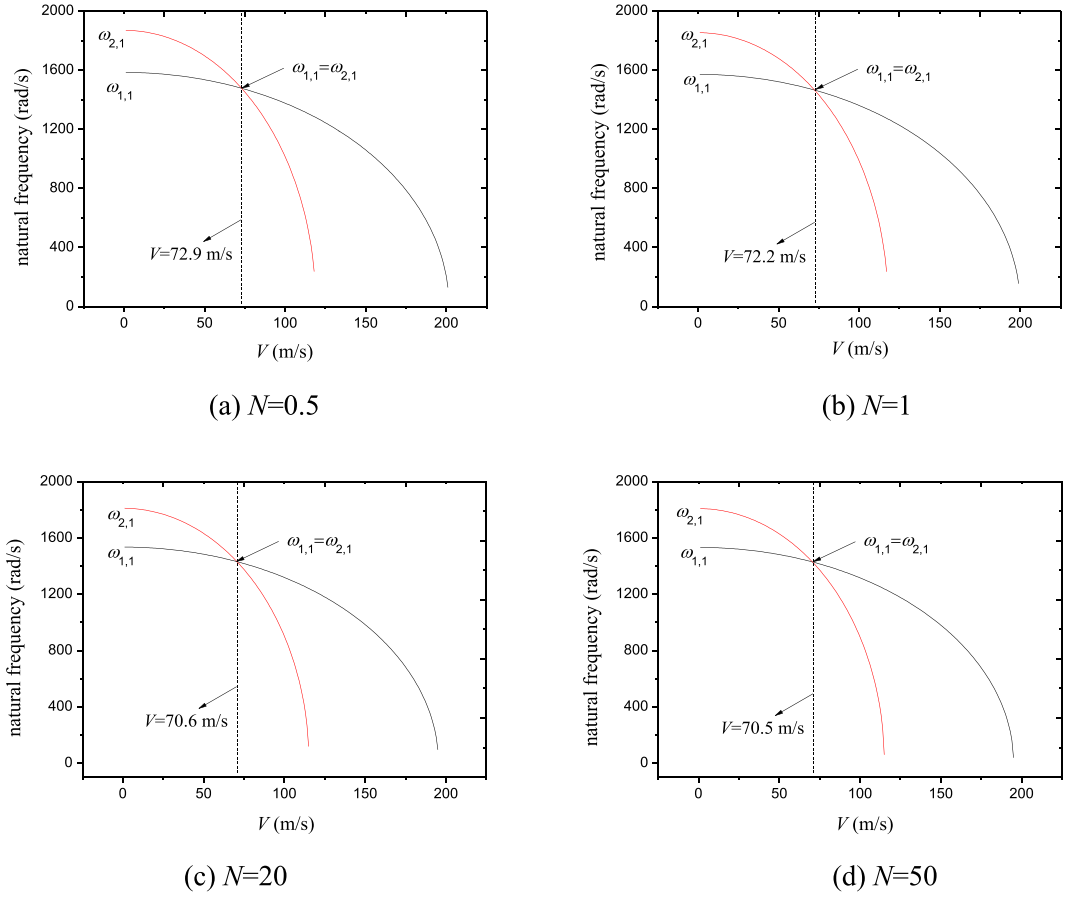


**Figure 2.** Variations of the first two natural frequencies against moving velocity for various power law exponents.

$$\dot{\mathbf{a}} = \mathbf{A}\mathbf{a} \tag{47}$$

in which **A** denote Jacobian matrix of the function **f** calculated in $\mathbf{a} = \mathbf{0}$.

For stable response, all real part of eigenvalues should be negative for the Jacobian matrix. Otherwise, the response is instable.

## Analytical and Numerical Results

To verify the present method, a comparison study is first made with the available reference for a simply supported stationary FGM plate made of $Si_3N_4$ and SUS304. The following parameters are used: $\mu = 0.28$, $a = 0.2$ m, $b = 0.2$ m and $h = 0.025$ m. The frequency parameter $\omega^* = \omega a^2/h\sqrt{\rho_m(1-\mu^2)/E_m}$ is calculated and compared with ref.[12], as shown in Table 1. One can find perfect agreement between these results has been achieved.

In what follows, we deal with a nickel/stainless-steel FGM plate that travels in the *x*-axis direction. At room temperature, material parameters of stainless steel are obtained as $E_S = 2.07788 \times 10^{11}\,\mathrm{Nm}^{-2}$, $\mu_S = 0.317756$ and $\rho_S = 8166\,\mathrm{kg\,m}^{-3}$, and those of nickel are obtained as $E_{Ni} = 2.05098 \times 10^{11}\,\mathrm{N\,m}^{-2}$, $\mu_{Ni} = 0.31$ and $\rho_{Ni} = 8900\,\mathrm{kg\,m}^{-3}$. *a*, *b* and *h* of the FGM plate are 0.4 m, 0.1 m and 0.001 m, respectively. It is clear this is a thin plate due to $b/h = 100$.

Figure 2 shows the change rule of the first two natural frequencies against moving velocity for a wide range of power-law exponents, i.e., $N = 0.5$ to $N = 50$. Here the pretension is set as $N_0 = 1000\,\mathrm{N/m}$; natural frequencies $\omega_{1,1}$

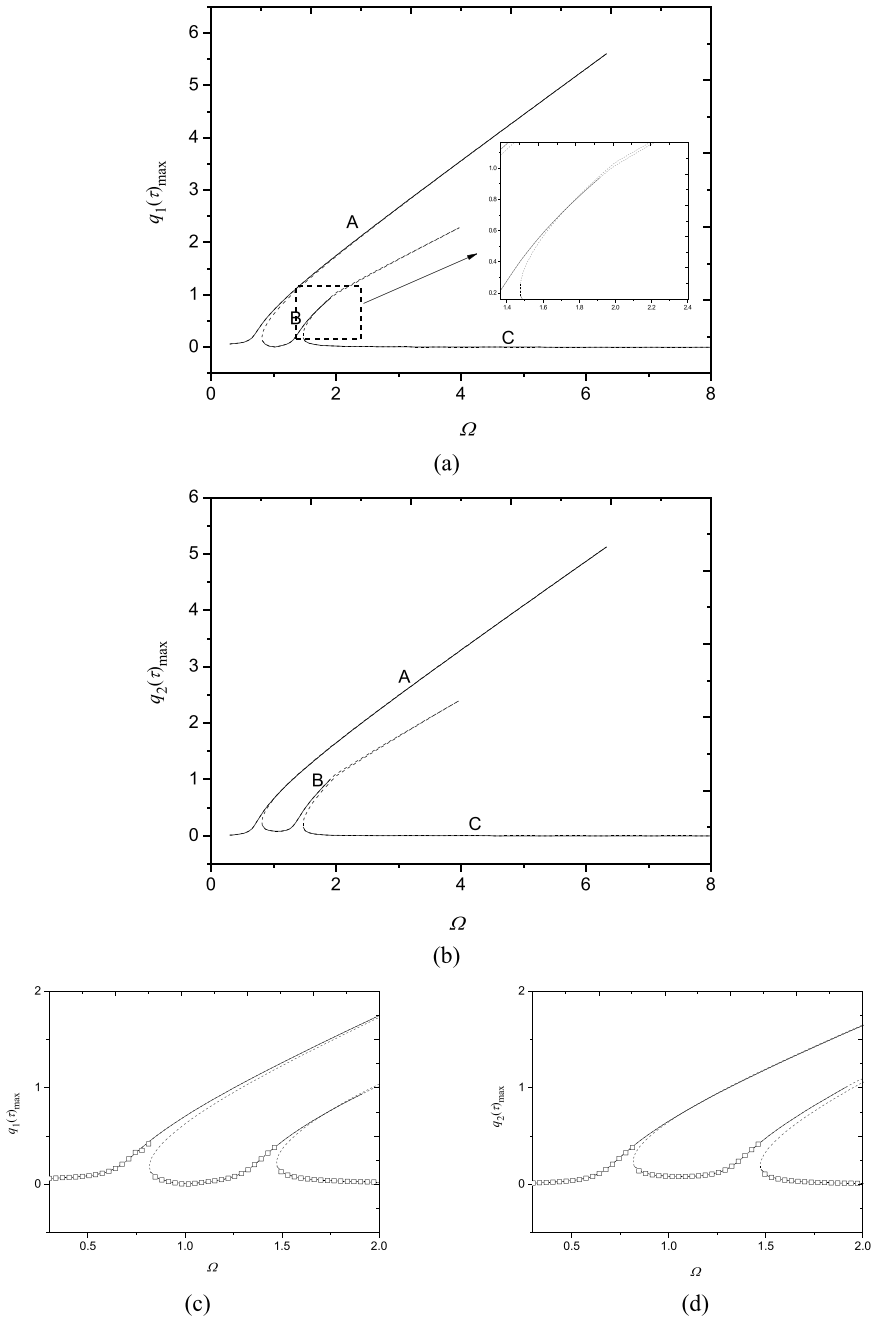


**Figure 3.** Frequency-response curves ($N_0 = 1000$ N/m, $F_0 = 10$N, $c = 10$ Ns/m$^3$, $N = 1$, $V = 72.2$ m/s): (**a**) maximum of $q_1(\tau)$; (**b**) maximum of $q_2(\tau)$; (**c**) magnification of (**a**); (**d**) magnification of (**b**). □, numerical solution; —, stable response; ---, unstable response.

and $\omega_{2,1}$ relate to the first mode ($\overline{m} = 1, \overline{n} = 1$) and second mode ($\overline{j} = 2, \overline{k} = 1$), respectively. From the figure, one may find that both $\omega_{1,1}$ and $\omega_{2,1}$ decrease with increasing moving speed of the FGM plate. However, their decrease rates are not always same. When the speed is small, i.e., $V < 20$ m/s, both decrease rates of the two frequencies have little difference. When $V > 20$ m/s, $\omega_{2,1}$ reduces quickly with the increase of moving speed; in contrast, $\omega_{1,1}$ still decreases slowly. This tendency results in the coincidence of these two natural frequencies at certain speeds, as seen in Fig. 2, and may result in 1:1 internal resonance. It is interesting to see that the coincidence of the lowest two natural frequencies appears under all of the considered power-law exponents. This demonstrates internal resonance exists in a broad range of constituent volume distribution in the moving FGM plate. In the present study, attention is mainly focused on this internal resonance behavior.

The frequency response relationships are investigated in Fig. 3 nearby the fundamental frequency. Here the parameters are $N_0 = 1000$ N/m, $F_0 = 10$ N, $c = 10$ Ns/m$^3$, $V = 72.2$ m/s and $N = 1$. The fundamental natural frequency is obtained as $\omega_{1,1} = 1464.61$ rad/s and the second natural frequency is $\omega_{2,1} = 1465.17$ rad/s. It is seen that the ratio of them is $\omega_{1,1}/\omega_{2,1} \approx 1$, which may give rise to the 1:1 internal resonance.

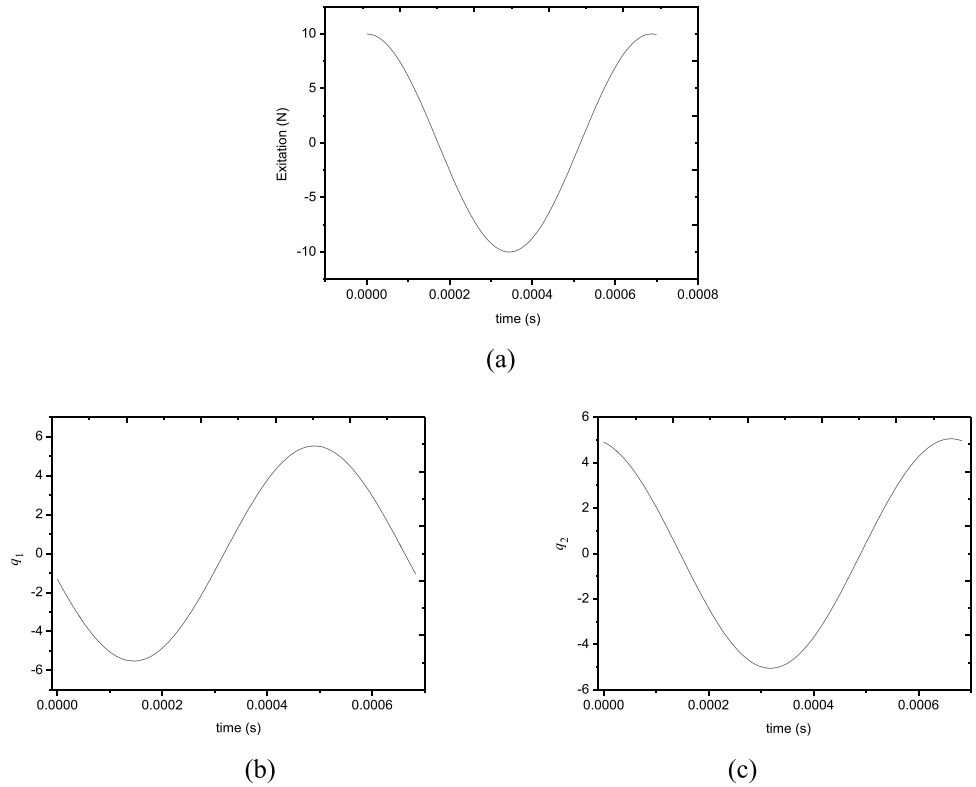


**Figure 4.** Time responses of generalized coordinates at $\Omega = 6.233$ in Fig. 3: (**a**) external excitation; (**b**) generalized coordinate $q_1$; (**c**) generalized coordinate $q_2$.

From Fig. 3(a,b), one may find that each generalized coordinates have two peaks and they are different from zero nearby the fundamental natural frequency, which demonstrates the first two modes are excited simultaneously owing to the nonlinear coupling through one-to-one internal resonance. These frequency-response relationships haven't been detected in moving homogenous plates before. Additionally, the frequency response curves exhibit hardening nonlinear characteristics. It is also seen that resonant amplitudes of each generalized coordinates are nearly same as each other due to 1:1 internal resonance. For the two peaks of each generalized coordinates, the first peak appears before the exact resonance condition $\Omega = 1$ and lasts to $\Omega = 6.3290$; the second one appears after $\Omega = 1$ and its resonance region is narrower than the first one. Each mode has three stable branches (A, B and C). There are two saddle-node bifurcations on the peak A, i.e., at $\Omega = 6.3290$ and $\Omega = 0.8272$. The resonant response loses its stability at the first bifurcation point and then recovers stability at the second bifurcation point. After that, the second stable peak B appears; this stable branch lasts to $\Omega = 1.9154$ and turns instable via Hopf bifurcation at this point. Coupled responses regain their stability at another bifurcation point at $\Omega = 1.4741$, resulting in the occurence of stable branch C. This branch relates to non-resonance response.

In order to verify the present analytical analysis, numerical solutions of Eq. (33) are solved by employing the Runge-Kutta method with assumed initial conditions $q_1(0) = q_2(0) = \dot{q}_1(0) = \dot{q}_2(0) = 0$. In Fig. 3(c,d), the analytical solutions are plotted together with numerical ones in a close-up view. It is seen that quite good agreement has been achieved between numerical and analytical solutions.

Figures 4 and 5 gives the time responses and phase locus of $q_1$ and $q_2$, where the excitation frequency is $\Omega = 6.233$. The excitation variation is shown in Fig. 4(a) for $F_0 = 10$ N. These figures show that the system response is periodic, and the amplitudes of both sides of the plate are symmetrical during a vibration period. Particularly, the amplitudes of each generalized coordinates are nearly the same but the phase angle is $\pi/2$.

Because power-law exponent is an important parameter which determines the configuration of FGM plates, its effect is particularly illuminated on vibration response of moving FGM plates in Fig. 6. As can be seen, power-law exponent has obvious influence on the resonance characteristics of FGM plates. When the power-law exponent rises, resonance amplitude of the plates increases accordingly. This is quite clear for the first peak in the frequency-response curves. Additionally, a trend is found that the second peak in the frequency-response curves shrinks with increasing power-law exponent.

Figure 7 shows frequency-response curves under a small excitation $F_0 = 2$N; the other parameters are kept the same as those in Fig. 3. As seen in Figs 3 and 7, both resonance amplitudes of the two modes decrease with the decreasing excitation amplitude. Also, as excitation amplitude decreases, hardening spring characteristics becomes weaker and weaker, and the resonance region gets narrower and narrower. It is worth noting that there still exist two obvious peaks on frequency response curves at very small excitation $F_0 = 2$N. This shows the 1:1 internal resonance in the present system can be excited easily even under extremely small excitation, indicating the sensibility of moving FGM plates to external excitation.

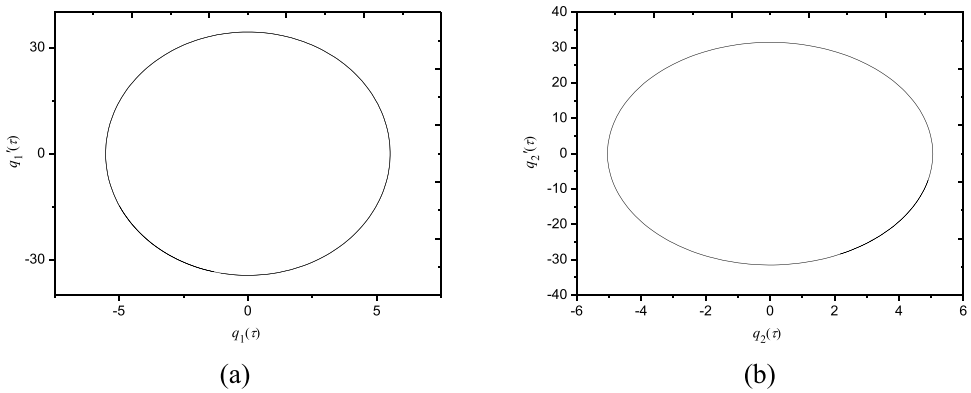


**Figure 5.** Phase plane diagram of generalized coordinates at $\Omega = 6.233$ in Fig. 3.

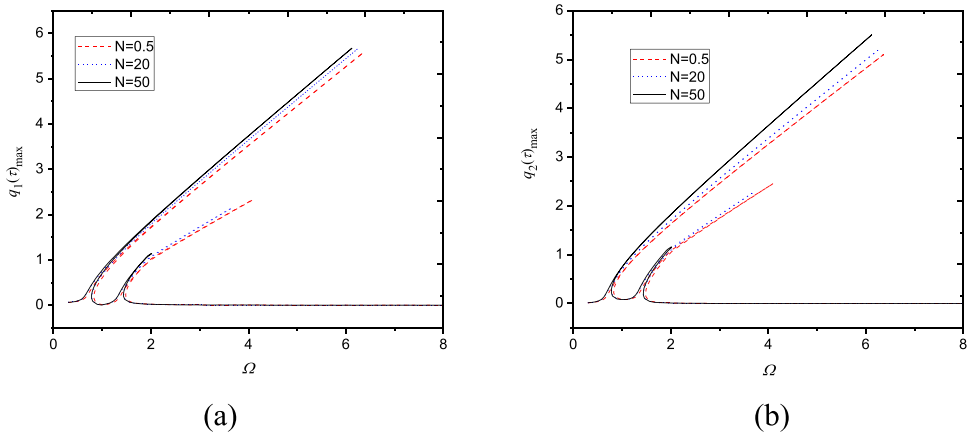


**Figure 6.** Effect of power-law exponent on frequency response of moving FGM plate ($N_0 = 1000$ N/m, $c = 10$ Ns/m$^3$, $V = 72$ m/s, $F_0 = 10$ N): (**a**) maximum of $q_1(\tau)$; (**b**) maximum of $q_2(\tau)$.

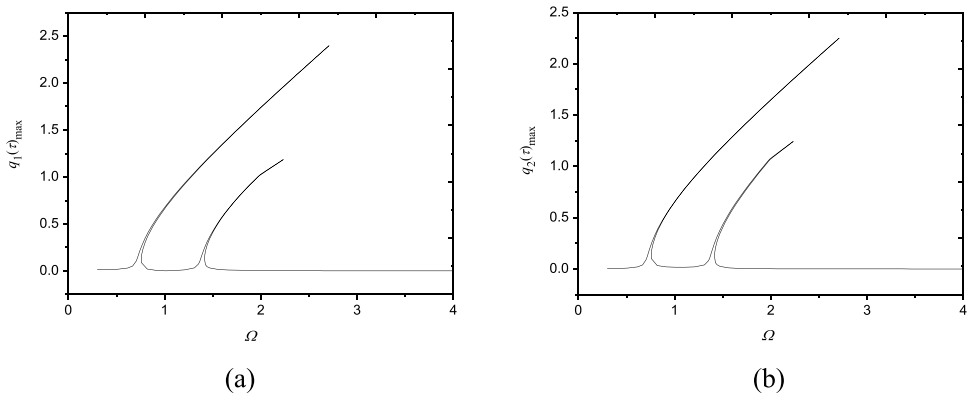


**Figure 7.** Frequency-response curves ($F_0 = 2$N, $V = 72.2$ m/s, $N = 1$, $c = 10$ Ns/m$^3$, $N_0 = 1000$ N/m): (**a**) maximum of $q_1(\tau)$; (**b**) maximum of $q_2(\tau)$.

Increasing the damping coefficient from $c = 10$ Ns/m$^3$ (Fig. 3) to $c = 50$ Ns/m$^3$, Fig. 8 is generated. Comparing Figs 3 and 8 reveals that the resonance region of the system narrows with the increase of damping coefficient. Moreover, the larger damping coefficient leads to the smaller resonant amplitudes of each mode. It is also found the 1:1 internal resonance phenomenon can happen even though the damping is very large, by contrast, the internal resonance has gone in composite shells with large damping coefficient[48].

Figures 9–11 show frequency response relationships of FGM plates with various power law exponents in a wide range (from $N = 0.5$ to 50). All these figures are plotted in the conditions of $\omega_{1,1}/\omega_{2,1} = 1$ for each power-law exponent to reveal the probable internal resonance phenomenon. The parameters used are shown under the

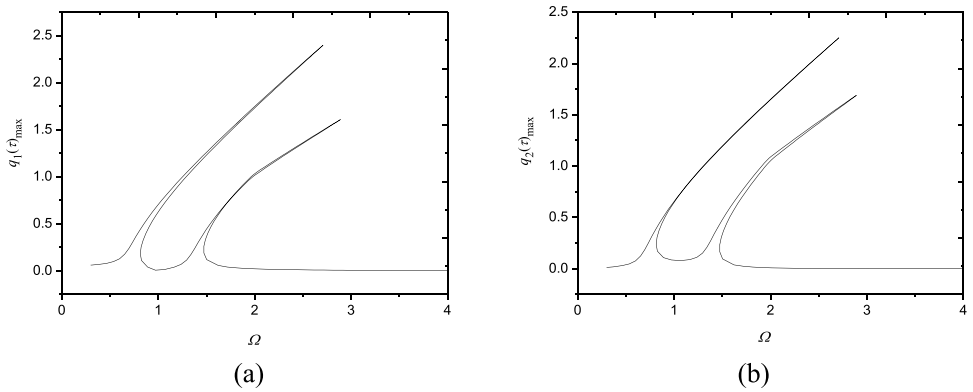


**Figure 8.** Frequency-response curves ($c = 50\,\text{Ns/m}^3$, $V = 72.2\,\text{m/s}$, $F_0 = 10\text{N}$, $N = 1$, $N_0 = 1000\,\text{N/m}$): (**a**) maximum of $q_1(\tau)$; (**b**) maximum of $q_2(\tau)$.

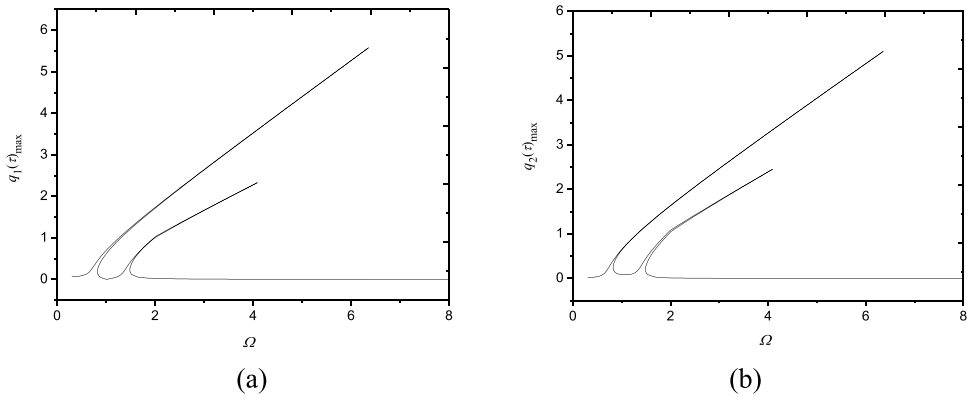


**Figure 9.** Frequency-response curves ($N = 0.5$, $N_0 = 10^3\,\text{N/m}$, $c = 10\,\text{Ns/m}^3$, $V = 72.85\,\text{m/s}$, $F_0 = 10\text{N}$): (**a**) maximum of $q_1(\tau)$; (**b**) maximum of $q_2(\tau)$.

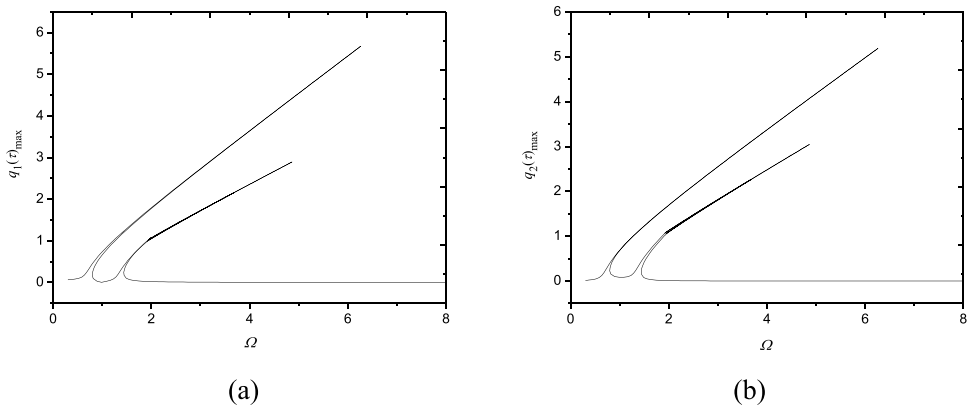


**Figure 10.** Frequency-response curves ($N = 20$, $N_0 = 10^3\,\text{N/m}$, $c = 10\,\text{Ns/m}^3$, $V = 70.61\,\text{m/s}$, $F_0 = 10\text{N}$): (**a**) maximum of $q_1(\tau)$; (**b**) maximum of $q_2(\tau)$.

corresponding figures. It is very interesting that 1:1 internal resonance appears in all these cases because each generalized coordinates generate extra peak. Comparing Figs 3, 9, 10 and 11 reveals that when the moving speed is within the range $V \in [70.5,\ 72.9]$, 1:1 internal resonance can happen in a wide range of power-law exponent in FGM plates. Therefore, this nonlinear phenomenon needs to be considered when designing and applying moving FGM plates.

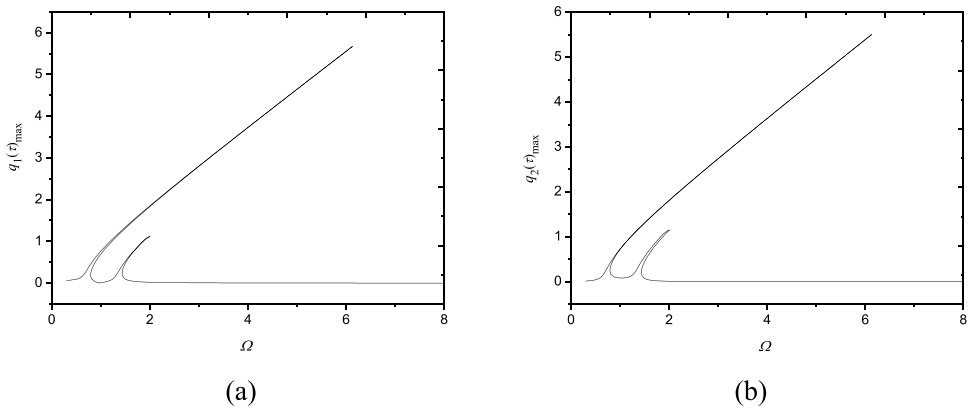


**Figure 11.** Frequency-response curves ($N = 50$, $N_0 = 10^3$ N/m, $c = 10$ Ns/m$^3$, $V = 70.47$ m/s, $F_0 = 10$N): (**a**) maximum of $q_1(\tau)$; (**b**) maximum of $q_2(\tau)$.

## Conclusions

A widespread one-to-one internal resonance phenomenon is detected in longitudinally moving FGM plates. On the base of d'Alembert's principle, the equation of transverse vibration is derived with the consideration of von Kármán's nonlinear geometrical relations. The approximately analytical analysis is conducted by using the Galerkin method together with the harmonic balance method. Results show that nonlinear frequency response relationship exhibits nonlinear hardening characteristics. The lowest two modes are excited simultaneously owing to the nonlinear coupling through one-to-one internal resonance. For moving FGM plates, the one-to-one internal resonance phenomenon may happen in a large range of constituent volume fraction. Furthermore, even extremely small excitation can excite this internal resonance.

## References


1. M. Koizumi, FGM activities in Japan, *Composites Part B: Engineering*. **28**, 1–4 (1997).
2. Swaminathan, K., Naveenkumar, D. T., Zenkour, A. M. & Carrera, E. Stress, vibration and buckling analyses of FGM plates—A state-of-the-art review. *Composite Structures*. **120**, 10–31 (2015).
3. Wang, Y. Q. & Zu, J. W. Large-amplitude vibration of sigmoid functionally graded thin plates with porosities. *Thin-Walled Structures*. **119**, 911–24 (2017).
4. Wang, Y. Q. & Zu, J. W. Nonlinear dynamic behavior of inhomogeneous functional plates composed of sigmoid graded metal-ceramic materials. *Science China Technological Sciences*. **61**, 1654–65 (2018).
5. Liu, D. Y., Wang, C. Y. & Chen, W. Q. Free vibration of FGM plates with in-plane material inhomogeneity. *Composite Structures*. **92**, 1047–51 (2010).
6. Ke, L.-L., Yang, J., Kitipornchai, S. & Bradford, M. A. Bending, buckling and vibration of size-dependent functionally graded annular microplates. *Composite Structures*. **94**, 3250–7 (2012).
7. Yang, C., Jin, G., Ye, X. & Liu, Z. A modified Fourier–Ritz solution for vibration and damping analysis of sandwich plates with viscoelastic and functionally graded materials. *International Journal of Mechanical Sciences*. **106**, 1–18 (2016).
8. Wang, Y. Q. & Zu, J. W. Vibration behaviors of functionally graded rectangular plates with porosities and moving in thermal environment. *Aerospace Science and Technology*. **69**, 550–62 (2017).
9. Wang, Y. Q. & Zu, J. W. Porosity-dependent nonlinear forced vibration analysis of functionally graded piezoelectric smart material plates. *Smart Materials and structures*. **26**, 105014 (2017).
10. Hao, Y. X., Zhang, W. & Yang, J. Nonlinear dynamics of a FGM plate with two clamped opposite edges and two free edges. *Acta Mechanica Solida Sinica*. **27**, 394–406 (2014).
11. Duc, N. D., Bich, D. H. & Cong, P. H. Nonlinear thermal dynamic response of shear deformable FGM plates on elastic foundations. *Journal of Thermal Stresses*. **39**, 278–97 (2016).
12. Alijani, F., Bakhtiari-Nejad, F. & Amabili, M. Nonlinear vibrations of FGM rectangular plates in thermal environments. *Nonlinear Dynamics*. **66**, 251–70 (2011).
13. Wang, Y. Q. & Zu, J. W. Speed-dependent nonlinear broadband vibrations of smart functionally graded piezoelectric material plates. *Journal of intelligent material systems and structures*. **29**, 1764–76 (2018).
14. Zhang, W., Yang, J. & Hao, Y. X. Chaotic vibrations of an orthotropic FGM rectangular plate based on third-order shear deformation theory. *Nonlinear Dynamics*. **59**, 619–60 (2010).
15. Allahverdizadeh, A., Oftadeh, R., Mahjoob, M. & Naei, M. Homotopy perturbation solution and periodicity analysis of nonlinear vibration of thin rectangular functionally graded plates. *Acta Mechanica Solida Sinica*. **27**, 210–20 (2014).
16. Yang, J., Hao, Y. X., Zhang, W. & Kitipornchai, S. Nonlinear dynamic response of a functionally graded plate with a through-width surface crack. *Nonlinear Dynamics*. **59**, 207–19 (2010).
17. Wang, Y. Q. & Zu, J. W. Nonlinear steady-state responses of longitudinally traveling functionally graded material plates in contact with liquid. *Composite Structures*. **164**, 130–44 (2017).
18. Wang, Y. Q., Huang, X. B. & Li, J. Hydroelastic dynamic analysis of axially moving plates in continuous hot-dip galvanizing process. *International Journal of Mechanical Sciences*. **110**, 201–16 (2016).
19. Sze, K. Y., Chen, S. H. & Huang, J. L. The incremental harmonic balance method for nonlinear vibration of axially moving beams. *Journal of Sound and Vibration*. **281**, 611–26 (2005).
20. Wang, Y. Q., Liang, L. & Guo, X. H. Internal resonance of axially moving laminated circular cylindrical shells. *Journal of Sound and Vibration*. **332**, 6434–50 (2013).
21. Panda, L. & Kar, R. Nonlinear dynamics of a pipe conveying pulsating fluid with combination, principal parametric and internal resonances. *Journal of Sound and Vibration*. **309**, 375–406 (2008).
22. Riedel, C. H. & Tan, C. A. Coupled, forced response of an axially moving strip with internal resonance. *International Journal of Non-Linear Mechanics*. **37**, 101–16 (2002).

23. Zhang, Y.-W., Yuan, B., Fang, B. & Chen, L.-Q. Reducing thermal shock-induced vibration of an axially moving beam via a nonlinear energy sink. *Nonlinear Dynamics.* **87**, 1159–67 (2017).
24. Ding, H. & Chen, L.-Q. Galerkin methods for natural frequencies of high-speed axially moving beams. *Journal of Sound and Vibration.* **329**, 3484–94 (2010).
25. Ding, H., Zhang, G.-C., Chen, L.-Q. & Yang, S.-P. Forced vibrations of supercritically transporting viscoelastic beams. *ASME Journal of Vibration and Acoustics.* **134**, 051007 (2012).
26. Yang, X.-D., Yang, S., Qian, Y.-J., Zhang, W. & Melnik, R. V. N. Modal Analysis of the Gyroscopic Continua: Comparison of Continuous and Discretized Models. *Journal of Applied Mechanics.* **83**, 084502 (2016).
27. Yang, X.-D., Zhang, W. & Melnik, R. V. N. Energetics and Invariants of Axially Deploying Beam with Uniform Velocity. *AIAA Journal.* **54**, 2181–7 (2016).
28. Ghayesh, M. H. Nonlinear forced dynamics of an axially moving viscoelastic beam with an internal resonance. *International Journal of Mechanical Sciences.* **53**, 1022–37 (2011).
29. Zhang, W. & Song, C. Higher-dimensional periodic and chaotic oscillations for viscoelastic moving belt with multiple internal resonances. *International Journal of Bifurcation and Chaos.* **17**, 1637–60 (2007).
30. Chen, L. Q. Analysis and control of transverse vibrations of axially moving strings. *Applied Mechanics Reviews.* **58**, 91–116 (2005).
31. Wang, Y., Du, W., Huang, X. & Xue, S. Study on the dynamic behavior of axially moving rectangular plates partially submersed in fluid. *Acta Mechanica Solida Sinica.* **28**, 706–21 (2015).
32. Wang, Y. Q. & Zu, J. W. Nonlinear dynamic thermoelastic response of rectangular FGM plates with longitudinal velocity. *Composites Part B: Engineering.* **117**, 74–88 (2017).
33. Hatami, S., Ronagh, H. & Azhari, M. Exact free vibration analysis of axially moving viscoelastic plates. *Computers & structures.* **86**, 1738–46 (2008).
34. Wang, Y. & Zu, J. W. Analytical analysis for vibration of longitudinally moving plate submerged in infinite liquid domain. *Applied Mathematics and Mechanics.* **38**, 625–46 (2017).
35. Banichuk, N., Jeronen, J., Neittaanmäki, P. & Tuovinen, T. On the instability of an axially moving elastic plate. *International Journal of Solids and Structures.* **47**, 91–9 (2010).
36. Marynowski, K. Free vibration analysis of the axially moving Levy-type viscoelastic plate. European. *Journal of Mechanics - A/Solids.* **29**, 879–86 (2010).
37. Wang, Y. Q. & Zu, J. W. Instability of Viscoelastic Plates with Longitudinally Variable Speed and Immersed in Ideal Liquid. *International Journal of Applied Mechanics.* **9**, 1750005 (2017).
38. Wang, Y. Q. & Yang, Z. Nonlinear vibrations of moving functionally graded plates containing porosities and contacting with liquid: internal resonance. *Nonlinear Dynamics.* **90**, 1461–80 (2017).
39. Wang, Y. Q., Xue, S. W., Huang, X. B. & Du, W. Vibrations of Axially Moving Vertical Rectangular Plates in Contact with Fluid. *International Journal of Structural Stability and Dynamics.* **16**, 1450092 (2016).
40. Loy, C. T., Lam, K. Y. & Reddy, J. N. Vibration of functionally graded cylindrical shells. *International Journal of Mechanical Sciences.* **41**, 309–24 (1999).
41. Wang, Y. & Zu, J. W. Nonlinear oscillations of sigmoid functionally graded material plates moving in longitudinal direction. *Applied Mathematics and Mechanics.* **38**, 1533–50 (2017).
42. Amabili, M. *Nonlinear vibrations and stability of shells and plates.* (New York: Cambridge University Press, 2008).
43. Wang, Y. Q. Electro-mechanical vibration analysis of functionally graded piezoelectric porous plates in the translation state. *Acta Astronautica.* **143**, 263–71 (2018).
44. Wang, Y. Q. & Zu, J. W. Nonlinear Dynamics of a Translational FGM Plate with Strong Mode Interaction. *International Journal of Structural Stability and Dynamics.* **18**, 1850031 (2018).
45. Wang, Y. & Zhang, Z. Non-Local Buckling Analysis of Functionally Graded Nanoporous Metal Foam Nanoplates. *Coatings.* **8**, 389 (2018).
46. Yang, X. D., Chen, L. Q. & Zu, J. W. Vibrations and stability of an axially moving rectangular composite plate. *Journal of Applied Mechanics.* **78**, 011018 (2011).
47. Wolfram, S. *The mathematica book.* Cambridge: (Cambridge university press, 1999).
48. Wang, Y. Q. Nonlinear vibration of a rotating laminated composite circular cylindrical shell: traveling wave vibration. *Nonlinear Dynamics.* **77**, 1693–707 (2014).


## Acknowledgements

This research was funded by the National Natural Science Foundation of China (Grant No. 11672188).

## Author Contributions

Yufei Zhang conceived the idea of this work. Yufei Zhang and Jintang Liu performed the theoretical analysis and the numerical simulation. Yufei Zhang wrote the manuscript.

## Additional Information

**Supplementary information** accompanies this paper at https://doi.org/10.1038/s41598-018-37921-9.

**Competing Interests:** The authors declare no competing interests.

**Publisher's note:** Springer Nature remains neutral with regard to jurisdictional claims in published maps and institutional affiliations.